Assignment of Red Antenna States in Photosystem I from *Thermosynechoccocus elongatus* by Single-Molecule Spectroscopy†

Marc Brecht,‡ Hauke Studier,‡ Alexandra F. Elli,§ Fedor Jelezko,§ and Robert Bittl*,‡

Fachbereich Physik, Freie Universität Berlin, Arnimalle 14, 14195 Berlin, Germany, and Physikalisches Institut, Universität Stuttgart, Pfaffenwaldring 57, 70569 Stuttgart, Germany

Received September 22, 2006; Revised Manuscript Received November 8, 2006

ABSTRACT: Single-molecule spectroscopy at cryogenic temperatures was used to elucidate spectral properties, heterogeneities, and dynamics of the chlorophyll *a* (Chla) molecules responsible for the fluorescence in photosystem I (PSI) from the cyanobacteria *Thermosynechoccocus elongatus*. Absorption and hole burning data suggest the presence of three pools absorbing at wavelengths greater than 700 nm with their absorption maxima at 708, 715, and 719 nm. The responsible Chla molecules are termed C708, C715, and C719. In the emission spectra of single PSI complexes, zero-phonon lines (ZPLs) were observed over the whole red emission range of PSI. The spectral region of the C708 pool is dominated by intense ZPLs; on the other hand, the broad emission of C715/C719 is unstructured and ZPLs are seen in this region much less frequently. Spectral jumps of ZPLs were observed. The dynamics as well as the spectral range covered by such jumps differ for C708 and C715/C719. This heterogeneity is likely caused by differences in the close environment of the chromophores. A tentative assignment of C708 and C715/C719 to Chla dimers and a Chla trimer is discussed, which is based on the remarkable structural differences in the environment of the most probable candidates for the red-most fluorescence.

In green plants, algae, and cyanobacteria, two transmembrane pigment−protein complexes are essential for light-driven oxygenic photosynthesis. This study focuses on photosystem I (PSI)[1] which transports, after photoexcitation, electrons from reduced plastocyanin or cytochrome c_6 on the luminal side to ferredoxin on the stromal side of the thylakoid membrane (*1*). The first step of the photosynthetic reaction is the absorption of a photon in the antenna system of PSI with subsequent energy transfer to the reaction center. At this point, the captured excitation energy is used to induce a transmembrane charge separation starting from a pigment with its main absorption at 700 nm (P700) (*1*, *2*).

The absorption spectra of PSI from green plants, algae, and cyanobacteria show the existence of Chla molecules absorbing at lower energy as the usual Q_y absorption at 680 nm of Chla in solution, and in particular at an excitation energy lower than that of the primary donor P700 (*3*, *4*). These red-shifted Chla's are often called the "red pool" or the "red-most" chlorophylls [for a review, see the work of Gobets et al. (*5*)]. Due to their spectral properties, Chla dimers have been discussed as candidates for the red pool Chla (e.g., ref *6*). If the excitation energy is localized within this red pool Chla, the stored energy is no longer sufficient to directly excite P700 to P700*. Additional activation energy, e.g., thermal energy of the phonon bath, is necessary to oxidize P700 and start the charge separation process. The question concerning the origin of the large red shift and the physiological role of the red pool is puzzling (*7*−*10*).

Even though the PSI complex from cyanobacteria differs in organization and content of polypeptides from those of higher plants and algae, it is used to investigate key properties of all types of PSI due to the existence of a well-resolved structural model for the cyanobacterium *Thermosynechoccocus elongatus* (previously *Synechoccocus elongatus*) from X-ray crystallography (*11*−*13*). From structural data, Krauss et al. (*14*) identified four putative candidates for the low-energy-absorbing Chla. One trimer and three dimers of Chla were selected. Even though the X-ray model at 2.5 Å resolution clearly shows the spatial arrangement of the ∼100 Chla's in PSI and their protein ligands (*11*, *14*), an unambiguous identification of the red pool Chla is impossible on the basis of the structural data alone. Although quantum chemical calculations are now able to reproduce the main features of the absorption spectrum for an individual Chla and also the bulk absorption spectrum from PSI (*7*, *15*, *16*), these methods are not yet able to describe the red-most Chla. It is necessary for this purpose to obtain more details about the electronic structure of these Chla's. Therefore, it is essential to use the advantages of each applicable spectroscopic method.

Detailed analysis of absorption spectra of *T. elongatus* allows the deconvolution of the red Chla into two pools (*17*−*20*). The pools have their main absorbance at 708 (C708) and 719 nm (C719). The distinction of two pools remains

† This work was supported by Volkswagenstiftung in the framework of the program "Physics, chemistry and biology with single molecules (I/77286, I/78361)".

* To whom correspondence should be addressed. E-mail: robert.bittl@physik.fu-berlin.de. Phone: ++49-30-838-56049. Fax: ++49-30-838-56046.

‡ Freie Universität Berlin.

§ Universität Stuttgart.

[1] Abbreviations: PSI, photosystem I; Chla, chlorophyll *a*; SMS, single-molecule spectroscopy; HB, hole burning; NPHB, nonphotochemical hole burning; FLN, fluorescence line narrowing; ZPL, zero-phonon line; PW, phonon wing; CS, conformational substates.

10.1021/bi061975k CCC: $37.00
Published on Web 12/29/2006

tentative because strong spectral overlap of the different bands exists (*17*). An additional red subpool (C715) was found by analysis of nonphotochemical hole burning (NPHB) spectra (*21*). Furthermore, this study showed similarities in the coupling of the chromophores with the surrounding protein scaffold between the C719 pool of *T. elongatus* and the C714 pool of *Synechocystis* PCC6803[2] (*22*).

Estimates for the number of Chla molecules involved in the red pool in *T. elongatus* have been deduced from the integrated absorbance at wavelengths longer than 700 nm. Zazubovich et al. (*21*) determined seven Chla's belong to the red pool (under the assumption of 96 Chla's in one PSI monomer), while Pålsson et al. (*17*, *23*) estimated there are nine to eleven Chla's (assuming 110 Chla's). Normalized to the total Chla content, these two estimates are in reasonable agreement.

Due to the unstructured shape of the bulk fluorescence spectra, it remains difficult to obtain detailed information about the spectral characteristics of the pools (*19*). This drawback can be avoided by use of site selective spectroscopic techniques like spectral hole burning (HB), fluorescence line narrowing (FLN) (*24*), and single-molecule spectroscopy (SMS) (*25*).

SMS serves as a method for avoiding ensemble averaging and thus can unravel information buried in spectra of large ensembles. SMS enables the observation of the emission of single chromophores (*26*). As a consequence, spectral features that are characteristic of single molecules become visible. At low temperatures, these are a narrow zero-phonon line (ZPL) and a broad phonon wing (PW). The ZPL belongs to an electronic transition without phonon creation or annihilation. The PW on the low-energy side of the ZPL is due to the interaction of the chromophore with its surrounding, leading to the excitation of phonons (lattice vibrational modes) (*27*).

The first single-molecule spectra of PSI at cryogenic temperature were recorded by Jelezko et al. (*28*). These experiments showed sharp emission lines at 705−715 nm assigned to ZPLs of Chla belonging to C708. No ZPLs were observed for C719. This effect was attributed to the stronger electron−phonon coupling for the latter pigments (*21*).

At room temperature and even at a low temperature (1.4 K), the emission of one chromophore is not fixed to a specific frequency, as shown by fluorescence excitation SMS on bacterial light-harvesting complex 2 (LH2) (*29*−*31*). The transition energy of ZPLs arising from LH2 varies in time, yielding line jumps on the nanometer scale as well as line broadening processes. This dynamics was explained in the framework of protein "energy landscapes" introduced by Frauenfelder (*32*). The high-dimensional energy surface of a protein is described in this picture by a hierarchy of conformational substates (CS). Usually, three main classes of CS, often called tiers, are discussed (*29*). The average height of the energy barriers between the CS is assumed to decrease from the upper to the lower tier. Changes between CS yield changes in the environment of embedded chromophores, which modify their electronic structure and induce the observed jumps in the absorption and emission frequency of ZPLs. The magnitudes of the observed spectral shifts in LH2 were assumed to represent the hierarchical organization of the energy tiers.

In this article, we show that the emission frequencies of ZPLs arising from C708 and C719 also undergo changes in time. While the spectral dynamics of the ZPLs from LH2 have been observed by fluorescence excitation spectroscopy, we record this dynamics directly by single-molecule fluorescence emission spectroscopy. The time scales of these spectral changes differ drastically for the C708, C715, and C719 pools. From this difference in dynamics, we conclude that the interaction of the chromophores of C708, C715, and C719 with the protein environment must be different. On the basis of the information from the X-ray structure (*11*, *14*), a tentative assignment is discussed.

MATERIALS AND METHODS

PSI from the cyanobacterium *T. elongatus* has been isolated as described in ref *33*. Purified PSI trimers were at first diluted in buffer (pH 7.5) containing 20 mM Tricine, 25 mM $MgCl_2$, and 0.4 mM detergent (β-DM, Sigma), to reach a Chla concentration of $\sim$20 μM. This amount of detergent is adequate for the critical solubilization concentration for a PSI trimer concentration of 0.5 μM to avoid PSI aggregation (*34*). For prereduction of P700, 5 mM sodium ascorbate was added. In further steps, this PSI-containing solution was diluted to a PSI trimer concentration of 3 pM. Less than 1 μL of this sample was placed between two cover slips, assuring spatial separation of individual PSI trimers. Sample preparation and mounting were accomplished under indirect daylight.

Experiments were carried out using a home-built confocal microscope operating at 1.4 K. For the imaging of single molecules, a scanning module (Galvoline GAL-1222 galvanometer scanner) was used to deflect the beams. The excitation source was a diode laser (676 nm $< \lambda <$ 688 nm, $\Gamma <$ 5 MHz over 20 s) (Sacher SYS-500-685-03, Littman Laser System). The fluorescence emission was focused either on an avalanche photodiode (Perkin-Elmer SPCM-AQR-15, $<$50 dark counts/s) for fast integral fluorescence detection or on an Acton Research $^1/_4$ m spectrograph (Acton SpectraPro308) equipped with a back-illuminated CCD camera (Roper Scientific Spec-10:100BR/LN) for recording whole fluorescence spectra at once. In a sequence of spectra, the usual exposure time for each spectrum is 1 s. The reaction time of the camera between two spectra in combination with laboratory-written acquisition software adds up to $\sim$0.15 s. To assess the polarization of these spectra, a Glen-Thomson polarizer (Newport) moved by a motorized rotation stage was positioned in front of the spectrograph. The stray light of the laser was blocked by a Raman long-pass filter (AHF). For illumination and detection, the same microscope objective (60$\times$, N.A. 0.85, Microthek) was employed and immersed in liquid helium. Typically, a laser intensity of $\sim$100 μW was used, yielding an excitation intensity in the focus on the order of 6×10^2 W/cm^2.

RESULTS

Single PSI complexes can be detected at low temperatures using the fluorescence emission of the red Chla (*28*). These molecules act at low temperatures as a trap for the excitation

[2] The red-most pool in *Synechocystis* PCC6803 has its main absorbance at 714 nm (C714).

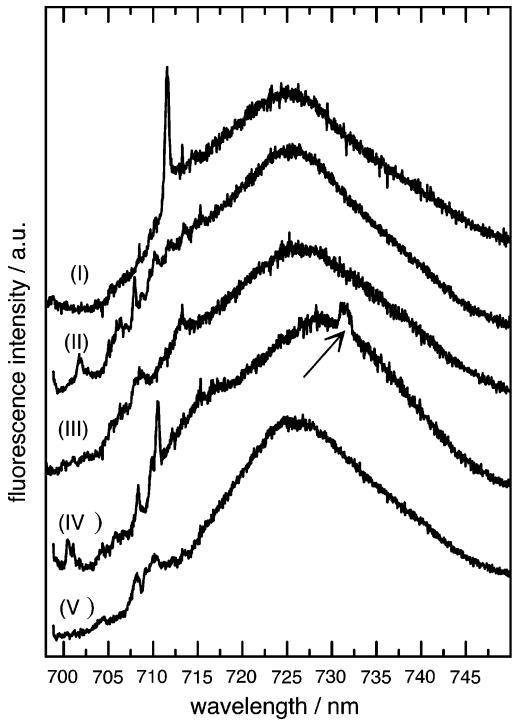

FIGURE 1: Single-molecule fluorescence emission spectra from PSI complexes of *T. elongatus*. Spectra were recorded on different individual complexes at 1.4 K. Excitation was at 680 nm, and the accumulation time was up to 300 s.

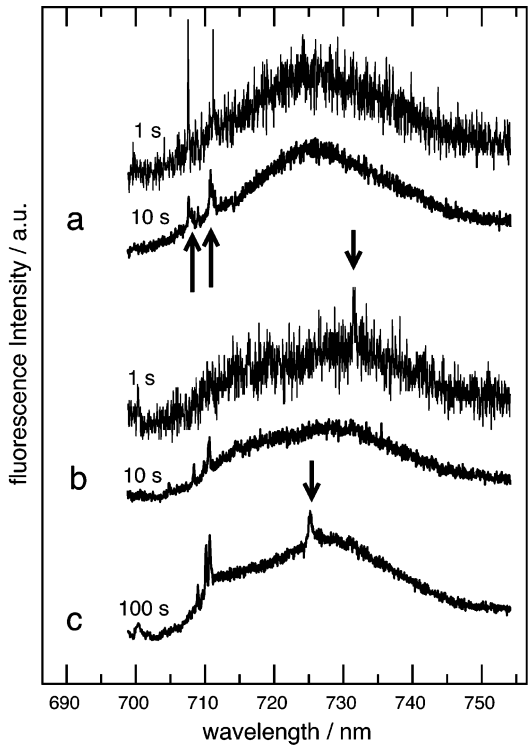

FIGURE 2: Dependence of fluorescence emission spectra of single PSI complexes on acquisition time. Spectra a and b were acquired in 1 and 10 s, as indicated. The accumulation time for spectrum c was 100 s. Spectra a−c arise from different complexes. The excitation wavelength was 680 nm, and $T = 1.4$ K.

energy and have a high fluorescence quantum yield. Figure 1 shows a selection of five fluorescence emission spectra (I−V) of single PSI complexes. The acquisition time for the spectra was up to 300 s. For better comparability, the spectra that exhibited intensity differences of ∼30% were scaled to a similar magnitude.

These spectra exhibit representative features and will each be described briefly. Spectrum I consists of a broad emission centered at 725 nm. In addition, a narrow intense line is observed at 711 nm with an accompanying shoulder stretching to 715 nm. We interpret this additional line as a ZPL (see below). In spectrum II, a very similar broad intensity distribution is observed. In the region between 700 and 717 nm, a number of additional peaks are found with less intensity compared to the intense ZPL at 711 nm in spectrum I. These lines exhibit no uniform line width and intensity. In spectrum III, again a broad emission with a maximum at 726 nm is observed. ZPLs are observed at 708 and 712 nm that are similar in shape and intensity. In spectrum IV, the broad intensity is shifted to 728 nm. Some additional features are present between 700 and 718 nm. They again differ in shape and intensity. Also in this spectrum, a line at 731 nm on the red wing of the broad intensity distribution is observed (denoted with an arrow). In spectrum V, the maximum of the broad emission is found at 725 nm and the additional peaks are found at 708 and 710 nm; due to their line width, these lines show a remarkable overlap.

All other recorded spectra exhibit a composition similar to those discussed above with the dominating broad intensity distribution and additional ZPLs. The maximum of the broad emission is found at 727 ± 2 nm. This value is slightly smaller than the intensity maximum at 730 nm determined for PSI in buffer diluted with glycerol (1:2, v/v) by conventional ensemble fluorescence spectroscopy at 4.2 K (*21*).

ZPLs are present in all spectra in the region below 717 nm, as shown in Figure 1. Some spectra exhibit narrow and intense ZPLs, and others exhibit only broadened lines with reduced intensity. The number of observed ZPLs is also variable. The line widths, γ, of the additional lines are in the range between 0.3 and 2 nm. Such line widths are much larger than the line width resulting solely from the dephasing time, T_2, of the optical transition. The spectral position of these lines as well as the line width and intensity shows variations from molecule to molecule. The intensity of the ZPLs compared with the overall intensity of the spectra remains in all cases below 10%.

The spectral region above 717 nm is broad and unstructured in the vast majority of the recorded spectra. Indications of ZPLs, like in spectrum IV, are rare in this spectral range.

A reduction of the line width of the additional lines could be achieved by a shortening the accumulation time for the spectra, as seen in Figure 2a. Both spectra of Figure 2a were recorded on the same molecule. The top spectrum was recorded within 1 s and the bottom within 10 s. The ZPLs at 707.6 and 711.2 nm (arrows in Figure 2a) have significantly different line widths. The line widths in the spectra taken at 1 and 10 s are ≤0.1 and ∼0.9 nm, respectively. The increase in the line width with an increase in accumulation time is a general feature observed for almost all the molecules that have been investigated. The value of ≤0.1 nm, as in the 1 s spectrum in Figure 2a, is close to the resolution of our setup (∼1 cm^{-1} $\hat{\approx}$ 0.05 nm). The experimental limit for the line width could not be achieved here, because the loss in the signal-to-noise ratio (S/N)

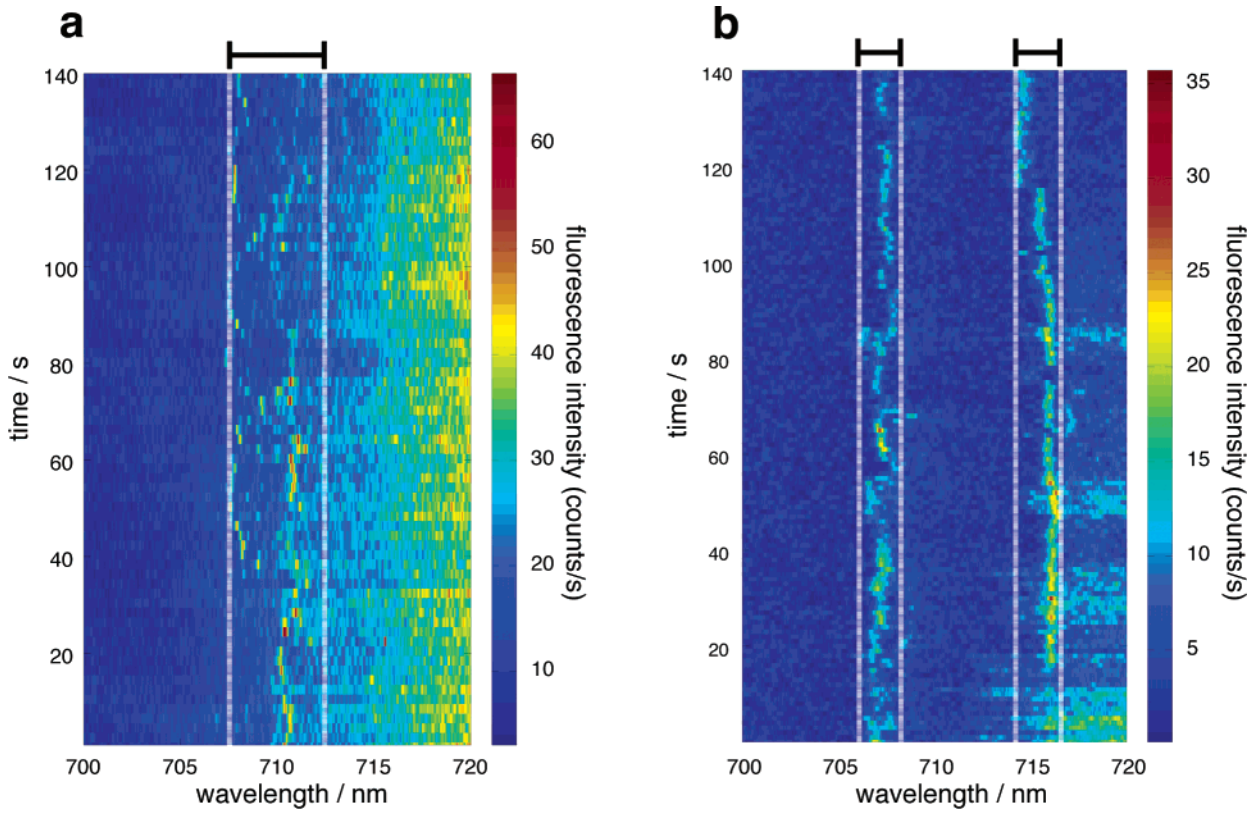

FIGURE 3: Plots of time-dependent fluorescence emission spectra of PSI. Time-dependent spectra for two different complexes are given (a and b). The time sequences of 140 spectra with an accumulation time of 1 s for each spectrum are displayed for both complexes. The white vertical dashed lines indicate the areas given in Figure 4 (see also the text). The excitation wavelength was 680 nm, and $T = 1.4$ K.

concomitant with a further decrease of the accumulation time prohibited a reliable identification of ZPLs.

In the spectral region above 717 nm, the dependence on the accumulation time has a different consequence for the observed lines. This is shown in Figure 2b. Again, both spectra were recorded with the same molecule. The top spectrum was recorded in 1 s and the bottom in 10 s. In the top 1 s spectrum, a narrow line is observed at 732 nm (denoted with an arrow). The intensity of this line is smaller than those observed in the region below 717 nm. Instead of a clearly visible line with an increasing width, this line is lost in the bottom 10 s spectrum. Using a longer accumulation time led to the disappearance of the far-red ZPLs in almost all observed PSI complexes. Even though weak ZPLs are rather common in spectra recorded within 1 s, significant lines with stable emission for times of $\gg$1 s remain an exception in the region above 717 nm. Of the investigated molecules, only two exhibited a stable line in this region. These are shown in Figures 1 (IV) and 2c; they were recorded in 100 and 261 s, respectively. The spectrum in Figure 2c shows a clearly visible line at 725 nm close to the maximum of the underlying broad intensity. The additional line shown in Figure 1 (IV) is located at 731 nm; this position is even lower in energy than the position of the maxima of the underlying broad intensity distribution.

In summary, we observe (i) spectra taken within 1 s yield in the region below 717 nm sharp ZPLs with line widths close to the resolution of the setup, (ii) in the region above 725 nm weak ZPLs can be observed, and (iii) an increase in the accumulation time beyond 1 s yields a broadening of the lines below 717 nm and mostly a disappearance of the weak lines in the far-red spectral range.

We found continuously recording spectra with a time resolution of 1 s to be the optimum choice for observing the spectral dynamics of ZPLs in our setup. To analyze the spectral dynamics of individual ZPLs, we recorded 42 arrays of time-dependent fluorescence spectra (td spectra) of single PSI complexes. Two of these arrays are presented in Figure 3 showing extreme examples of the dynamical behavior of the ZPLs in the spectral range between 705 and 717 nm. Trails representing the emission of ZPLs can be seen in both arrays over the whole period of data accumulation (140 s). In the left array, ZPLs arise in the region between 707 and 713 nm. Above 715 nm, the intensity increases due to the onset of the broad emission band. The spectral trail formed by the ZPL is dominated by remarkable spectral jumps. Within 1 s, this ZPL changes its position by up to 4 nm. The behavior of the ZPL shown in the picture suggests the existence of discrete spectral positions. These positions were taken successively along the spectral trail. The number of spectral positions taken by the ZPL during the observation time is large. In some spectra of the given array, two or more spectral positions can be found. Two explanations for this finding will be discussed later.

The ZPLs visible in the right array behave differently. The span of their spectral dynamics is remarkably smaller. While the two trails in Figure 3b have a very similar dynamical range, they differ substantially in their dynamic properties. The left trail ($\sim$707 nm) can be grossly characterized by diffusion-like sampling of the whole covered range. However, closer inspection shows, as for the ZPL in Figure 3a, preferred spectral positions occupied for longer times and discrete jumps. The right trail ($\sim$715 nm) exhibits initially rather stable emission at a narrow wavelength range around

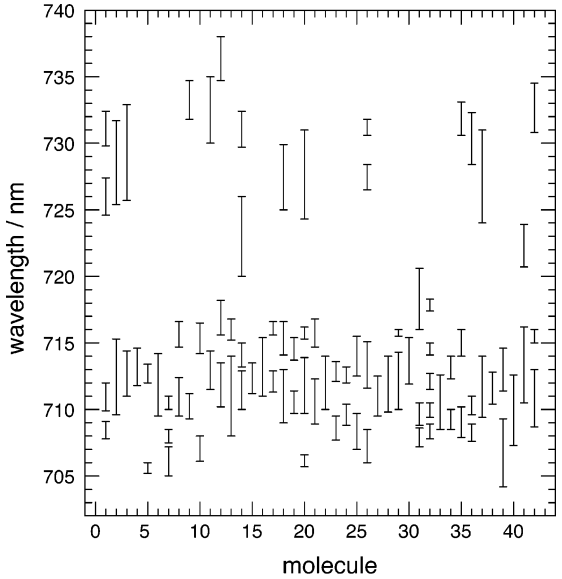

FIGURE 4: Statistical analysis of the distribution of ZPLs. The chart shows the individual regions in which ZPLs were observed in the td spectra of 42 individual PSI complexes. The determination of these areas from the td spectra is explained in the text and visualized in Figure 3.

716 nm with small variations on the 0.3 nm scale. With increasing times, the line shifts in a few jumps toward 714 nm. The rate of the observed spectral jumps was found to be dependent on the intensity of the excitation light, indicating that photoexcitation is at least partially responsible for the activation of the protein dynamics (*35*).

Irrespective of these differences in their dynamics, all recorded td spectra show that within the time window of our measurements the emission range covered by the observed ZPLs is restricted to defined spectral areas on the nanometer scale. White dashed lines illustrate these areas in Figure 3. The range in panel a spans from 707.3 to 712.6 nm. The ranges in panel b are, as discussed above, smaller than that in panel a and span only from 706.1 to 708.0 nm and from 714.2 to 716.5 nm. The corresponding areas have been determined for all of the 42 arrays recorded on different individual PSI complexes and are shown in Figure 4 as bars.

The areas determined from the spectra given in Figure 3 can be found at position 40 (a) and 10 (b) in Figure 4. The td spectra of each PSI show an individual dynamic behavior of their ZPLs. The spectral ranges occupied by the spectral trails of the ZPLs are in some cases well-separated, and in some cases, these ranges overlap. In the case where well-separated spectral ranges were observed, the determined areas represent the dynamic region of one ZPL (see, e.g., numbers 7, 20, and 32; Figure 4); the maximum were five separated areas (number 32; Figure 4). Consequently, one broad range is given in the case where the spectral ranges of the ZPLs overlap (see, e.g., numbers 3, 6, and 37; Figure 4). Therefore, the number of areas given in Figure 4 is not directly correlated with the number of emitters responsible for the ZPLs in the spectra.

Inspection of Figure 4 reveals two well-separated bands of areas covered by ZPLs. One band is formed in the region below 717 nm and one above 725 nm. First, we want to focus on the wavelength region below 717 nm. From the representation given in Figure 4, it becomes evident that some ZPLs reside in more extended and some in more restricted areas. Extended areas can be found, e.g., for molecules 13, 40, and 41. More confined areas were observed, e.g., for molecules 7, 23, 24, and 32. For most molecules, one or two regions are visible in this spectral band.

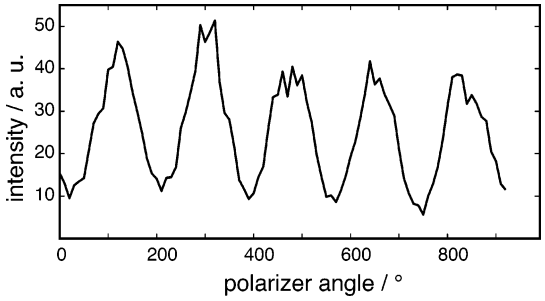

FIGURE 5: Integrated fluorescence intensity of the emission of a single PSI complex in the range from 732 to 736 nm as a function of the polarizer angle. Spectra were recorded in steps of 10°.

ZPLs responsible for the band above 725 nm were observed only in the td spectra of 14 molecules. Compared to those ZPLs in the region below 717 nm, those above 725 nm are lower in intensity, and their spectral trails are in most cases only partially traceable.

To obtain additional details about the number of emitters responsible for the fluorescence emission of a single PSI, the polarization of the emission was analyzed. Elli et al. (*36*) recently performed such an analysis for the ZPLs in the region below 715 nm. There, a small number of emitters were deduced from the high degree of polarization. Here we investigated the polarization of the broad mainly unstructured emission above 725 nm. The polarization dependence of the integrated fluorescence intensity emitted in the region of 732−736 nm of a single PSI is shown in Figure 5. Note that the given polarizer angle is defined with respect to an arbitrary laboratory axis and is uncorrelated with the polarization of the excitation light. The data indicate a high degree of polarization of the emitted light. Therefore, the emission in this spectral range arises either from a number of chlorophylls with parallel transition dipole moments or from a very small number of emitting states.

DISCUSSION

The spectroscopic characteristics of the fluorescence emission of single PSI complexes can be separated into two sections. The first section concerns the spectral range below 717 nm and the second the range above 717 nm. In the following, their spectroscopic characteristics are discussed separately.

The fluorescence emission of the Chla molecules associated with C708 is expected at ∼710 nm. The emission spectra (Figure 2) exhibit lines that differ in shape, position, and intensity in this region. Such lines were first observed by Jelezko et al. (*28*) in emission as well as in excitation spectra of single PSI complexes, and they were assigned to ZPLs of Chla molecules of C708 (*28*, *37*, *38*). The strong time dependence of the line width shows that spectral diffusion is the main broadening process (Figure 3).

All these ZPLs should be accompanied by a PW. The shape of these PWs is determined by the distribution of the protein phonons and strength of the electron phonon coupling. The phonon distribution is centered at 20−30 cm^{-1} and has a width of ∼30 cm^{-1} (*27*). The ratio between the

intensity emitted in the ZPL (I_{ZPL}) and in the PW (I_{PW}) is related via the Huang−Rhys factor, *S*, defined by the relation $\exp(-S) = I_{ZPL}/(I_{ZPL} + I_{PW})$ (*39*). However, the intensity of the PW remains below the S/N in our setup. This can be rationalized as follows. The Huang−Rhys factor for C708 (of *T. elongatus* and *Synechocystis* PCC6803) was found to be larger than that of monomeric antenna Chla (*21*), and an *S* value of 1.2−1.3 was determined for *Synechocystis* PCC6803 (*37*, *38*). Using this value, we calculate an intensity ratio between the maxima of the ZPL and the PW phonon wing of ∼20. Even when the limited spectral resolution is taken into account, this intensity ratio is too small for an identification of a PW at the given S/N, in agreement with the experimental observation.

The movement of the ZPLs from C708 is characterized by discrete spectral jumps over the nanometer range and not by continuous changes in their position (Figure 4). Since these jumps happen on the time scale of our time resolution (1 s), it is impossible to uniquely explain the occurrence of multiple ZPLs in the spectra acquired in 1 s. The straightforward interpretation would be to assign the different ZPLs to different emitting states within one observed PSI trimer. However, the different lines can as well arise from one emitting state with jumps between discrete emission wavelengths on a subsecond time scale.

An explanation of the spectral dynamics observed in LH2 is given in ref *29* based on the hierarchy of tiers in the energy landscape of a protein (*32*). We adopt this explanation for the observed spectral dynamics in PSI.

High energetic barriers between the different conformational substates characterize the highest tier in the energy landscape. Under the given low-temperature condition, the barriers cannot be crossed and the system rests in one given conformational substate in the first tier. The energetic barriers between the different substates within the second tier are lower, and these barriers can be crossed under the experimental conditions. The crossing of these barriers induces the observed spectral jumps. The jumps of the spectral position often reach the nanometer scale (Figure 3a). The spectral ranges that can be accessed by the individual members of C708 within the second tier are shown in Figure 4. These are similar for the C708 pool to the values given for LH2 (∼50 cm^{-1}). The substates of the third hierarchical tier are again embedded in those of the second tier. The energetic barriers between the different states within the third hierarchical level are lower than those of the second tier. Like in LH2, evidence of this tier is found in the line widths of the ZPLs. The observed line width exceeds always the expected values of a stationary ZPL. This broadening is independent of the line jumping associated with the crossing of the barriers in the second tier. Therefore, the rate of the associated conformational changes must be much higher.

Although the shape of the energy landscape differs for all PSI complexes, the organization in these hierarchical tiers is maintained. The resulting spectral ranges from single PSI complexes cover only a part of the whole spectral band of C708. The collection of all spectral ranges from the analyzed PSI complexes in Figure 4 shows how the inhomogeneous broadened band observed in bulky samples is built up by single complexes.

The shape of the fluorescence emission of single PSI complexes above 717 nm remains unstructured for most PSI complexes (Figure 1). The fluorescence emission spectra taken with a rotating polarizer in the front of the spectrograph indicate a high degree of polarization of the emitted light in the region above 717 nm (Figure 5). Strong polarization was observed also for all other investigated PSI complexes. A strong polarization of the emitted light requires either a single emitter as the origin of the emission or a number of emitters with parallel transition dipole moments. Because the PSI complexes in our samples are randomly oriented, it is unlikely that the transition moments of several emitters would appear to be parallel in all cases. Therefore, the number of emitters responsible for this broad and intense emission in this spectral region is again low, and a small number of individual emitters are expected.

On the basis of an *S* value of 2.2, a γ of 0.5 cm^{-1}, and phonon frequencies ω_1 and ω_2 of 30 and 110 cm^{-1}, respectively (*21*), found for C719 of *T. elongatus*, we calculate an intensity ratio of the maxima of the ZPL and the PW of ∼7. Therefore, ZPLs should also be present in the spectral range above 717 nm. However, almost no corresponding ZPL was found in the range between 717 and 725 nm, and only very rarely were ZPLs observed above 725 nm. Instead, we usually observe a broad unstructured emission. Decreasing the intensity of the ZPLs below the intensity of the phonon wing would require an increase in the intrinsic γ or of *S* beyond the largest values of ∼3 reported by FLN (*40*). Therefore, another broadening mechanism must render the ZPLs of C715 and C719 invisible. Most likely, these are rapid spectral diffusion processes that broaden the ZPLs on the nanometer scale within 1 s. Thus, the rate of conformational changes close to the chromophores of C715 and C719 yielding changes in the nanometer range must be remarkably enhanced compared to C708. Because virtually no ZPL is observed in the range between 717 and 725 nm, it is likely that on average the spectral dynamics is faster in this range than above 725 nm. The spectral range between 717 and 725 nm covers the range expected for the emission of C715, and the fluorescence above 725 nm is probably due to C719. Therefore, we find the fastest spectral dynamics for C715, followed by C719, and, finally, the slowest spectral dynamics for C708. This, in turn, implies that the chromophores of C708 must face an environment with the lowest flexibility and C715 an environment allowing the highest flexibility.

The four putative candidates for the low-energy-absorbing Chla identified from structural data consists of one trimer and three dimers of Chla (*11*, *12*). The trimer consists of Chla molecules B33, B32, and B31 (in the notation of ref *11*) and is located at the lumenal side of subunit PsaB. One of the dimers (A32−B7) is close to the trimerization domain; the other two dimers are on the stromal side of the membrane, one in subunit PsaA (A38−A39) and one in subunit PsaB (B37−B38) close to the interface of PsaA and PsaB. The inspection of the important interaction range of ∼4.5 Å (*41*) between chromophore and protein revealed clear differences in the binding situation of those four candidates. The two A38−A39 and B37−B38 dimers are not tightly bound to the protein. Only one Chla per dimer is directly coordinated by His at the side of the Mg ion, and only one possible partner for a hydrogen bridge with the keto group of the fifth ring of the Chla is found for each dimer. In contrast, the B7−A32 dimer is more tightly bound to the protein. Both

Mg ions are directly coordinated, one by a His and one by a Gln, and both Chla molecules possess a partner for a hydrogen bond to the keto group. The B31−B32−B33 trimer is coordinated at the Mg ion of B31 with a His. The other Chla's are possibly coordinated at the Mg ion via water molecules (*7*). A partner of a hydrogen bond to the keto group is found only for B32.

The different binding situations of the four candidates yield different degrees of flexibility. The presented spectra show that the time scale of the spectral diffusion is slowest for C708. Therefore, we tentatively assign C708 to the more tightly bound B7−A32 dimer. For C715 and C719, faster spectral diffusion is found. The A38−A39 and B37−B38 dimers are less tightly bound than the B7−A32 dimer but more tightly bound than the B31−B32−B33 trimer. Therefore, the A38−A39 and B37−B38 dimers, which are close to the reaction center, are good candidates for C719 as well as for C714 in *Synechocystis* PCC6803 (*42*). The environment of the B31−B32−B33 trimer allows even more flexibility than all three dimers. Therefore, it is tempting to assign this trimer to C715. The assignment of C715 to the B31−B32−B33 trimer is supported by the supposed nonexistence of this trimer in *Synechocystis* PCC6803, where a corresponding pool like C715 was not found (*22*).

ACKNOWLEDGMENT

We thank E. Schlodder (TU Berlin, Berlin, Germany) for the PSI samples and helpful discussion.

REFERENCES

1. Brettel, K. (1997) Electron transfer and arrangement of the redox cofactors in photosystem I, *Biochim. Biophys. Acta 1318*, 322−373.
2. Brettel, K., and Leibl, W. (2001) Electron transfer in photosystem I, *Biochim. Biophys. Acta 1507*, 100−114.
3. Gobets, B., Ericsson, M., Palsson, L., Shubin, V., Karapetyan, N., van Grondelle, R., and Dekker, J. (1996) Site selected polarized fluorescence spectroscopy of photosystem I particles isolated from the cyanobacteria *Spirulina platensis*, *Prog. Biophys. Mol. Biol. 65*, PE221−PE221.
4. Palsson, L. O., Flemming, C., Gobets, B., van Grondelle, R., Dekker, J. P., and Schlodder, E. (1998) Energy transfer and charge separation in photosystem I: P700 oxidation upon selective excitation of the long-wavelength antenna chlorophylls of *Synechococcus elongatus*, *Biophys. J. 74*, 2611−2622.
5. Gobets, B., and van Grondelle, R. (2001) Energy transfer and trapping in photosystem I, *Biochim. Biophys. Acta 1507*, 80−99.
6. Melkozernov, A. N., Lin, S., and Blankenship, R. E. (2000) Femtosecond transient spectroscopy and excitonic interactions in Photosystem I, *J. Phys. Chem. B 104*, 1651−1656.
7. Sener, M. K., Lu, D. Y., Ritz, T., Park, S., Fromme, P., and Schulten, K. (2002) Robustness and optimality of light harvesting in cyanobacterial photosystem I, *J. Phys. Chem. B 106*, 7948−7960.
8. Rivadossi, A., Zucchelli, G., Garlaschi, F. M., and Jennings, R. C. (1999) The importance of PSI chlorophyll red forms in light-harvesting by leaves, *Photosynth. Res. 60*, 209−215.
9. Gobets, B., van Stokkum, I. H., van Mourik, F., Dekker, J. P., and van Grondelle, R. (2003) Excitation wavelength dependence of the fluorescence kinetics in Photosystem I particles from *Synechocystis* PCC 6803 and *Synechococcus elongatus*, *Biophys. J. 85*, 3883−3898.
10. Bruggemann, B., Sznee, K., Novoderezhkin, V., van Grondelle, R., and May, V. (2004) From structure to dynamics: Modeling exciton dynamics in the photosynthetic antenna PS1, *J. Phys. Chem. B 108*, 13536−13546.
11. Jordan, P., Fromme, P., Witt, H. T., Klukas, O., Saenger, W., and Krauss, N. (2001) Three-dimensional structure of cyanobacterial photosystem I at 2.5 Å resolution, *Nature 411*, 909−917.
12. Fromme, P., Jordan, P., and Krauss, N. (2001) Structure of photosystem I, *Biochim. Biophys. Acta 1507*, 5−31.
13. Ben-Shem, A., Frolow, F., and Nelson, N. (2003) Crystal structure of plant photosystem I, *Nature 426*, 630−635.
14. Krauss, N., Schubert, W. D., Klukas, O., Fromme, P., Witt, H. T., and Saenger, W. (1996) Photosystem I at 4 Å resolution represents the first structural model of a joint photosynthetic reaction centre and core antenna system, *Nat. Struct. Biol. 3*, 965−973.
15. Sundholm, D. (2003) A density-functional-theory study of bacteriochlorophyll b, *Phys. Chem. Chem. Phys. 5*, 4265−4271.
16. Sundholm, D. (2000) Comparison of the electronic excitation spectra of chlorophyll a and pheophytin a calculated at density functional theory level, *Chem. Phys. Lett. 317*, 545−552.
17. Pålsson, L., Dekker, J., Schlodder, E., Monshouwer, R., and van Grondelle, R. (1996) Polarized site-selective fluorescence spectroscopy of the long-wavelength emitting chlorophylls in isolated Photosystem I particles of *Synechococcus elongatus*, *Photosynth. Res. 48*, 239−246.
18. Byrdin, M., Rimke, I., Schlodder, E., Stehlik, D., and Roelofs, T. A. (2000) Decay kinetics and quantum yields of fluorescence in photosystem I from *Synechococcus elongatus* with P700 in the reduced and oxidized state: Are the kinetics of excited state decay trap-limited or transfer-limited? *Biophys. J. 79*, 992−1007.
19. Gobets, B., van Amerongen, H., Monshouwer, R., Kruip, J., Rögner, M., van Grondelle, R., and Dekker, J. (1994) Polarized site-selected fluorescence spectroscopy of isolated photosystem-I particles, *Biochim. Biophys. Acta 1188*, 75−85.
20. Frese, R. N., Palacios, M. A., Azzizi, A., van Stokkum, I. H., Kruip, J., Rögner, M., Karapetyan, N. V., Schlodder, E., van Grondelle, R., and Dekker, J. P. (2002) Electric field effects on red chlorophylls, β-carotenes and P700 in cyanobacterial Photosystem I complexes, *Biochim. Biophys. Acta 1554*, 180−191.
21. Zazubovich, V., Matsuzaki, S., Johnson, T., Hayes, J., Chitnis, P., and Small, G. (2002) Red antenna states of photosystem I from cyanobacterium *Synechococcus elongatus*: A spectral hole burning study, *Chem. Phys. 275*, 47−59.
22. Hsin, T. M., Zazubovich, V., Hayes, J. M., and Small, G. J. (2004) Red antenna states of PSI of cyanobacteria: Stark effect and interstate energy transfer, *J. Phys. Chem. B 108*, 10515−10521.
23. Pålsson, L., Gobets, B., Fleming, C., Ericsson, L., van Grondelle, R., Schlodder, E., and Dekker, J. (1996) Long-wavelength antenna pigments in photosystem I, *Prog. Biophys. Mol. Biol. 65*, PE217−PE217.
24. Purchase, R., Bonsma, S., Jezowski, S., Gallus, J., Konz, F., and Volker, S. (2005) The power of line-narrowing techniques: Applications to photosynthetic chromoprotein complexes and autofluorescent proteins, *Opt. Spectrosc. 98*, 699−711.
25. Tamarat, P., Maali, A., Lounis, B., and Orrit, M. (2000) Ten years of single-molecule spectroscopy, *J. Phys. Chem. A 104*, 1−16.
26. Kiraz, A., Ehrl, M., Brauchle, C., and Zumbusch, A. (2003) Low temperature single molecule spectroscopy using vibronic excitation and dispersed fluorescence detection, *J. Chem. Phys. 118*, 10821−10824.
27. Jankowiak, R., Hayes, J. M., and Small, G. J. (1993) Spectral hole-burning spectroscopy in amorphous molecular-solids and proteins, *Chem. Rev. 93*, 1471−1502.
28. Jelezko, F., Tietz, C., Gerken, U., Wrachtrup, J., and Bittl, R. (2000) Single-molecule spectroscopy on photosystem I pigment-protein complexes, *J. Phys. Chem. B 104*, 8093−8096.
29. Hofmann, C., Aartsma, T. J., Michel, H., and Kohler, J. (2003) Direct observation of tiers in the energy landscape of a chromoprotein: A single-molecule study, *Proc. Natl. Acad. Sci. U.S.A. 100*, 15534−15538.
30. Rutkauskas, D., Novoderezkhin, V., Cogdell, R. J., and van Grondelle, R. (2004) Fluorescence spectral fluctuations of single LH2 complexes from *Rhodopseudomonas acidophila* strain 10050, *Biochemistry 43*, 4431−4438.
31. Novoderezhkin, V. I., Rutkauskas, D., and van Grondelle, R. (2006) Dynamics of the emission spectrum of a single LH2 complex: Interplay of slow and fast nuclear motions, *Biophys. J. 90*, 2890−2902.
32. Frauenfelder, H., Wolynes, P. G., and Austin, R. H. (1999) Biological physics, *Rev. Mod. Phys. 71*, S419−S430.
33. Fromme, P., and Witt, H. T. (1998) Improved isolation and crystallization of Photosystem I for structural analysis, *Biochim. Biophys. Acta 1365*, 175−184.

34. Müh, F., and Zouni, A. (2005) Extinction coefficients and critical solubilisation concentrations of photosystems I and II from *Thermosynechococcus elongatus*, *Biochim. Biophys. Acta 1708*, 219−228.
35. Ketelaars, M., Segura, J. M., Oellerich, S., de Ruijter, W. P. F., Magis, G., Aartsma, T. J., Matsushita, M., Schmidt, J., Cogdell, R. J., and Kohler, J. (2006) Probing the electronic structure and conformational flexibility of individual light-harvesting 3 complexes by optical single-molecule spectroscopy, *J. Phys. Chem. B 110*, 18710−18717.
36. Elli, A. F., Jelezko, F., Tietz, C., Studier, H., Brecht, M., Bittl, R., and Wrachtrup, J. (2006) Red pool chlorophylls of photosystem I of the cyanobacterium *Thermosynechococcus elongatus*: A single-molecule study, *Biochemistry 45*, 1454−1458.
37. Hayes, J., Matsuzaki, S., Ratsep, M., and Small, G. (2000) Red chlorophyll a antenna states of photosystem I of the cyanobacterium *Synechocystis* sp. PCC 6803, *J. Phys. Chem. B 104*, 5625−5633.
38. Ratsep, M., Johnson, T., Chitnis, P., and Small, G. (2000) The red-absorbing chlorophyll a antenna states of photosystem I: A hole-burning study of *Synechocystis* sp. PCC 6803 and its mutants, *J. Phys. Chem. B 104*, 836−847.
39. Huang, K., and Rhys, A. (1950) Theory of light absorption and non-radiative transitions in F-centres, *Proc. R. Soc. London, Ser. A 204*, 406−423.
40. Ihalainen, J., Ratsep, M., Jensen, P., Scheller, H., Croce, R., Bassi, R., Korppi-Tommola, J., and Freiberg, A. (2003) Red spectral forms of chlorophylls in green plant PSI: A site-selective and high-pressure spectroscopy study, *J. Phys. Chem. B 107*, 9086−9093.
41. Lesch, H., Schlichter, J., Friedrich, J., Vanderkooi, J. M. (2004) Molecular probes: What is the range of their interaction with the environment? *Biophys. J. 86*, 467−472.
42. Melkozernov, A. N., Lin, S., and Blankenship, R. E. (2000) Excitation dynamics and heterogeneity of energy equilibration in the core antenna of photosystem I from the cyanobacterium *Synechocystis* sp. PCC 6803, *Biochemistry 39*, 1489−1498.

BI061975K